Experimental Determination of the $H_2SO_4/HNO_3/H_2O$ Phase Diagram in Regions of Stratospheric Importance

Keith D. Beyer,* Anne R. Hansen, and Nick Raddatz

Department of Chemistry, Wisconsin Lutheran College, 8800 West Bluemound Road, Milwaukee, Wisconsin 53226

Received: June 4, 2003; In Final Form: November 22, 2003

We have investigated the region of the $H_2SO_4/HNO_3/H_2O$ ternary liquid/solid phase diagram bounded by ice, nitric acid trihydrate (NAT), and sulfuric acid tetrahydrate (SAT) using differential scanning calorimetry and IR spectroscopy of thin films. We report measurements and analysis of the eutectic melting curves in the ternary system of the hydrates mentioned as well as the temperature of the eutectics ice/SAT/NAT, ice/sulfuric acid hemihexahydrate (SAH)/NAT, and SAT/NAT. We report for the first time an analysis of the content of the solid phase of completely frozen samples and find that sulfuric acid octahydrate (SAO) is often present in frozen ternary samples and can be a significant portion of the solid phase. We provide a description of how the melting path of a frozen ternary sample can be predicted using the ternary phase diagram. We have parametrized our melting point data and provide equations to generate the ternary melting surface. Finally, we compare our results to the historic work of Carpenter and Lehrmann (Carpenter, C. D.; Lehrman, A. *Trans. AIChE* **1925**, *17*, 35) to other more recent work and to the output of the Aerosol Inorganics Model.

Introduction

Polar stratospheric clouds (PSCs) play a crucial role in the depletion of ozone (O_3).[1,2] PSCs have been discussed in terms of three types: Ia (composed primarily of solid particles produced from a ternary mixture of $H_2SO_4/HNO_3/H_2O$); Ib (liquid particles consisting of a ternary mixture of $H_2SO_4/HNO_3/H_2O$); and II (water−ice).[3,4] In the case of type Ia, it is believed that nucleation of one (most likely nitric acid trihydrate, NAT) or more solids in the ternary liquid particles occurs, which leads to condensation of background vapors on the particles at temperatures 2−4 K above the frost point of water−ice. This leads these newly solid particles to grow to a size where they can sediment to lower regions in the stratosphere.[5−7] Laboratory experiments have shown that specific solids are thermodynamically stable under these conditions,[8,9] and field measurements have shown solid particle formation is the most likely explanation for observations of very large particles.[10−13] It has been shown by various laboratory studies summarized by DeMore et al.[14] that the surface reaction probability of stratospheric gases depends on the nature of the surface; therefore, it is critical to know the phase diagrams of the various acid hydrates accurately.

Only one comprehensive experimental study of the $H_2SO_4/HNO_3/H_2O$ liquid/solid phase diagram has been performed, that of Carpenter and Lehrman in 1925.[15] Their study was performed before discovery of the binary solids sulfuric acid octahydrate (SAO),[16,17] sulfuric acid hemihexahydrate (SAH),[17] sulfuric acid trihydrate (SATri),[18] and nitric acid dihydrate (NAD).[19,20] Thus, their analysis did not include these solids in the ternary phase diagram. However, they did map regions of stability for the following solids: ice, NAT, nitric acid monohydrate (NAM), HNO_3, sulfuric acid tetrahydrate (SAT), sulfuric acid dihydrate (SAD), sulfuric acid monohydrate (SAM), H_2SO_4, and a ternary solid $10SO_3{\cdot}N_2O_5{\cdot}9H_2O$, which others have assigned to the binary solid $5H_2SO_4{\cdot}HNO_3$.[21] Their analysis included tables of the final melting temperature in each primary phase region as well as a plot of phase boundaries separating these regions. As far as we can determine, no systematic study to identify temperatures and compositions of either phase boundaries or ternary eutectics was undertaken by Carpenter and Lehrman. Two recent studies report data useful in constructing the ternary phase diagram. Molina et al.[8] show DSC thermograms for two ternary solutions from which melting data can be garnered. Chang et al.[22] report melting points for ternary samples that have one or five weight percent sulfuric acid for nitric acid concentrations 0−35 wt %. In the case of 5 wt % H_2SO_4 samples, they report observing ternary eutectic transitions but do not report temperature values. Fox et al.[23] report the existence of a new hydrate, $H_2SO_4{\cdot}HNO_3{\cdot}5H_2O$, based on vapor pressure measurements of ternary samples. Finally, many researchers have studied the freezing behavior of ternary samples, both aerosols and bulk, with the aim of applying laboratory results to polar stratospheric clouds.[9,24−28] However, these studies have not reported data useful in determining the ternary phase diagram; they have focused on the conditions of solid formation in ternary samples, not eutectic, phase boundary, or final melting temperatures.

In the experiments described here, we have reinvestigated the $H_2SO_4/HNO_3/H_2O$ solid/liquid phase diagram in the region formed by drawing an Alkemade line between NAT and SAT, which includes the stability regions of ice, SAO, SAH, SAT, and NAT. An Alkemade line is "a straight line connecting the composition points of two phases whose primary phase fields share a common boundary curve."[29] This region includes many probable solution concentrations of ternary stratospheric particles as calculated from the model of Carslaw et al.[30] The ternary solid proposed by Fox et al.[23] and one of the samples studied by Molina et al.[8] lie outside this region and thus were not studied

* Author to whom correspondence may be addressed. E-mail: Keith_Beyer@wlc.edu.

10.1021/jp035572v CCC: $27.50 © 2004 American Chemical Society
Published on Web 01/13/2004

in this work. We have, however, incorporated our recent work on the HNO_3/H_2O[31] and H_2SO_4/H_2O[32] systems as binary components of the ternary phase diagram.

Experimental Section

Sample Preparation. Acid samples were prepared by diluting 98 wt % ACS reagent grade H_2SO_4 and 68.5 wt % ACS reagent grade HNO_3 supplied by Fischer with Culligan purified water. The concentrated acids were standardized by acid−base titration, and the concentration of all samples is known to ± 0.40 wt %.

Infrared Spectra. The sample cell used for infrared spectra is shown schematically and explained in detail in previous literature.[23] Briefly, a small drop of ternary solution was placed between two AgCl windows, which were held in the center of an aluminum block by a threaded metal ring. Sample volumes were 1−2 μL. On each side of the aluminum block a Pyrex cell was purged with dry nitrogen gas. KBr windows were placed on the end of each cell, sealed with O-rings and held in place by metal clamps. Heat tape was wrapped around the purge cells to prevent condensation on the KBr windows. The sample was cooled by immersing the end of the aluminum block in liquid nitrogen and warmed by resistive heaters connected to a temperature controller. Temperature was measured by a copper/constantan thermocouple placed at the edge of the AgCl windows and connected to the temperature controller. The temperature of the cell was calibrated using Culligan purified water and high-purity organic solvents (Aldrich): decane, octane, and acetic anhydride of which the melting points are 243.5, 216.4, and 200.2 K, respectively.[33] The IR cell temperatures are known on average to within ±1.3 K, i.e., a temperature we measured in the IR cell of a specific transition is within 1.3 K of the transition temperature we measure (of the same transition) using the differential scanning calorimeter (DSC).

Spectra were obtained with a Mattson Instruments Galaxy 4020 FTIR with 16 cm^{-1} resolution. Each spectrum is the average of 4 scans. Before spectra were taken of a sample, a background scan was obtained from a dry, purged sample cell. Samples were cooled to 192 K at 3 K per minute and then allowed to warm to room temperature without resistive heating, typically this was 1 K/minute. If acid samples did not freeze while cooling, they were held at 145 K for up to an hour and the samples would crystallize upon warming. In all cases, our spectra compare well for ice, SAH, SAT, SAO, and NAT with those previously published.[19,20,32,34]

Differential Scanning Calorimeter. Thermal data was obtained with a Mettler Toledo DSC 822e with liquid nitrogen cooling. Industrial grade nitrogen gas was used as a purge gas with a flow rate of 50 mL per minute. The temperature reproducibility of this instrument is better than ±0.05 K. Our accuracy is estimated to be ±0.9 K with a probability of 0.94 based on a three-point temperature calibration[35] using indium, HPLC grade water, and anhydrous, high-purity (99%+) octane from Aldrich, the latter two stored under nitrogen. The sensitivity of our instrument to thermal signals is high. Previously, we have calculated our sensitivity to detecting a component undergoing a thermal transition to be <50 ppm by mass.[31]

Samples were contained in a 30 μL platinum pan and typically had a mass of approximately 25 mg. In cases where samples did not freeze upon repeated runs, we used larger samples ranging from 60 to 120 mg contained in 70-μL platinum pans. Each sample was weighed before and after the experiment using a Mettler-Toledo AT20 microgram balance. The average mass loss from evaporation during the experiment was less than 1%. A typical sample was cooled to 173 K at 10 K per minute, held at that temperature for 30 min, warmed to 190 K at 10 K per minute and held there for 30 min, warmed at a rate of 1 K per minute until 278 K, and then finally to 298 K at 10 K per minute. In cases where samples did not completely freeze (especially near the ternary eutectics), various other methods were attempted: holding at 183 K for 12 h, holding at 190 K for longer periods, and warming at 0.5 K per minute. None of these methods were seen to induce complete freezing.

Results

Phase Diagram. The ice/SAT/NAT Alkemade region of the ternary phase diagram is shown in Figure 1, which shows all the sample concentrations we studied in our experiments. A total of 161 samples were studied; of those, 126 appeared to completely freeze as evidenced by a melting transition at the ternary eutectic temperature. Figure 2 shows the temperature contours for this system determined from the final melting temperatures as well as the phase boundary curves. The complete set of experimental final melting points for the $H_2SO_4/HNO_3/H_2O$ samples as well as our experimental melting points for the HNO_3/H_2O[31] and H_2SO_4/H_2O[32] systems used to create Figure 2 are given in Table 1S in Supporting Information. Thermograms for four ternary samples noted by colored dots in Figure 2 are given in Figure 3. Boundary curve temperatures and compositions shown in Figures 1 and 2 were determined by plotting final melting temperatures as a function of one of the three concentrations while holding a second concentration constant. The melting points were then fit to second-order polynomials on each side of the phase boundary and the resulting equations solved simultaneously for the phase boundary composition and temperature. The resulting phase boundary temperatures and compositions are listed in Table 1. An example of this procedure is shown in Figure 4 where we have plotted final melting temperatures of samples as a function of nitric acid concentration for the constant sulfuric acid concentrations given in the figure. At zero percent sulfuric acid, the plot is simply that of the nitric acid/water binary system. The two solids represented by the liquidous surfaces are ice and NAT on the left and right side of the phase boundary, respectively. It is easily seen that as the concentration of H_2SO_4 is increased, the ice/NAT phase boundary moves to lower HNO_3 concentrations and decreases in temperature. This phenomenon is the result of the phase boundary roughly following a line of constant water concentration from 0/33/67 to 25/8/67 $H_2SO_4/HNO_3/H_2O$ wt %, respectively (see Figure 2). At this point, the phase boundary curves and briefly follows a constant HNO_3 concentration of about 3 wt %. Here it intersects both the ice/SAH eutectic (stable) and ice/SAT eutectic (metastable), each forming a unique ternary eutectic point at the intersection of three phase boundaries. As the phase boundary continues toward less water content, it intersects the SAH/SAT peritectic curve forming a tributary reaction point (not shown in the figures). Finally, the phase boundary terminates in this subsystem as the SAT/NAT eutectic at approximately 42/15/43 $H_2SO_4/HNO_3/H_2O$ wt % and a temperature of 231.75 K. An example thermogram for a solution that displayed the SAT/NAT eutectic is given in Figure 3 (red trace).

We have parametrized the melting points in the ice and NAT primary phase fields using second-order polynomial fits to the data as a function of both HNO_3 and H_2SO_4 concentrations, respectively. In the ice region, the parametrization using constant HNO_3 compositions and varying H_2SO_4 composition continuously ("NA") reproduced our experimental melting points to

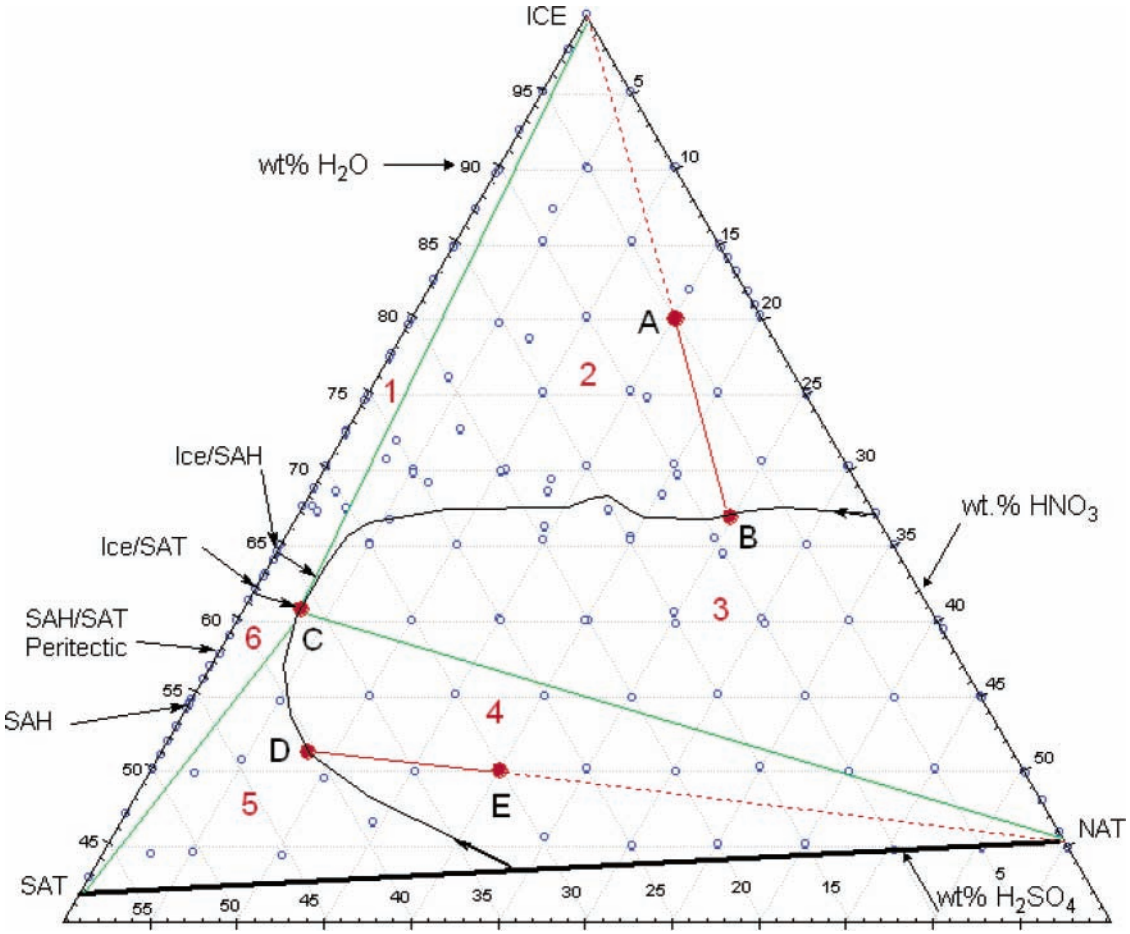

Figure 1. Ice/SAT/NAT region of the $H_2SO_4/HNO_3/H_2O$ phase diagram. Blue points are concentrations of samples we investigated (blue points exist under red dots at points A and E). Arrows on the diagram indicate direction of decreasing temperature along the phase boundaries (black curves). Black line between SAT and NAT composition is an Alkemade line. Red numbers, dots, lines, and green lines are explained in the text.

within ±0.53 K. The parametrization using constant H_2SO_4 composition and varying HNO_3 composition continuously ("SA") performed worse, reproducing our experimental data to within ±2.04 K. We then used the coefficients from the NA parametrization and parametrized them as a function of HNO_3 using second- and third-order polynomials to determine if one equation as a function of both HNO_3 and H_2SO_4 concentrations could be generated. This parametrization reproduced our experimental data to within ±1.65 K. Since this is significantly worse than the error in our experimental data, we abandoned this approach. Similarly, in the NAT region, we generated an NA and an SA parametrization and each reproduced our experimental data to within ±0.28 and ±0.20 K, respectively. The combined parametrized equation again reproduced our data with much greater uncertainty than our experimental error. Therefore, we report the polynomial coefficient values for the NA parametrization in the ice primary phase field in Table 2 and the NA and SA parametrization coefficients in the NAT primary phase field in Tables 3 and 4, respectively. The concentration ranges for which the equations are valid are also given in each respective table. We included both equations in the NAT region because they cover slightly different concentration ranges but together cover essentially the entire NAT region. The parameters given in the table are for the polynomial

$$T = A_2x^2 + A_1x + A_0 \quad (1)$$

where T is the melting temperature in Kelvin and x is the wt % of H_2SO_4 in the NA equations and the wt % of HNO_3 in the SA equation, respectively. We have not parametrized the SAT primary phase field of the phase diagram. This region is a very small fraction of this Alkemade subregion of the phase diagram. Additionally, solutions were very difficult to freeze in this region; thus, we have very few experimental melting points to use in a parametrization, making such an equation unreliable for reproducing the data.

Ternary Eutectics. Knowledge of the composition and temperature of the ternary eutectics, ice/SAH/NAT and ice/SAT/NAT, is very important to determine the conditions under which a completely frozen ternary sample will melt. Because of the difficulty in completely freezing a ternary sample with compositions at or near the ternary eutectic, we were unable to determine the specific composition of either ternary eutectic but have determined (in agreement with Carpenter and Lehrman) the probable composition of each eutectic. Our ternary eutectic points shown in Figure 2 are arrived at following trends in the final melting points in the regions of these eutectics and from knowing the ice/SAH and ice/SAT binary eutectics. Simply, a line was drawn from the binary ice/SAH and ice/SAT eutectics, respectively, toward the NAT composition point on the HNO_3/H_2O axis, ending at the intersection of the ice/NAT boundary curve.

With respect to the ice/SAT/NAT eutectic, it is expected that this eutectic will occur at a temperature below that of the ice/SAT eutectic at 199.32 K[32] since NAT would represent an impurity to the binary eutectic, thus lowering the melting point as a result of the change in the chemical potential of the system. In our experiments, we observed a melting signal at 197.4 ±

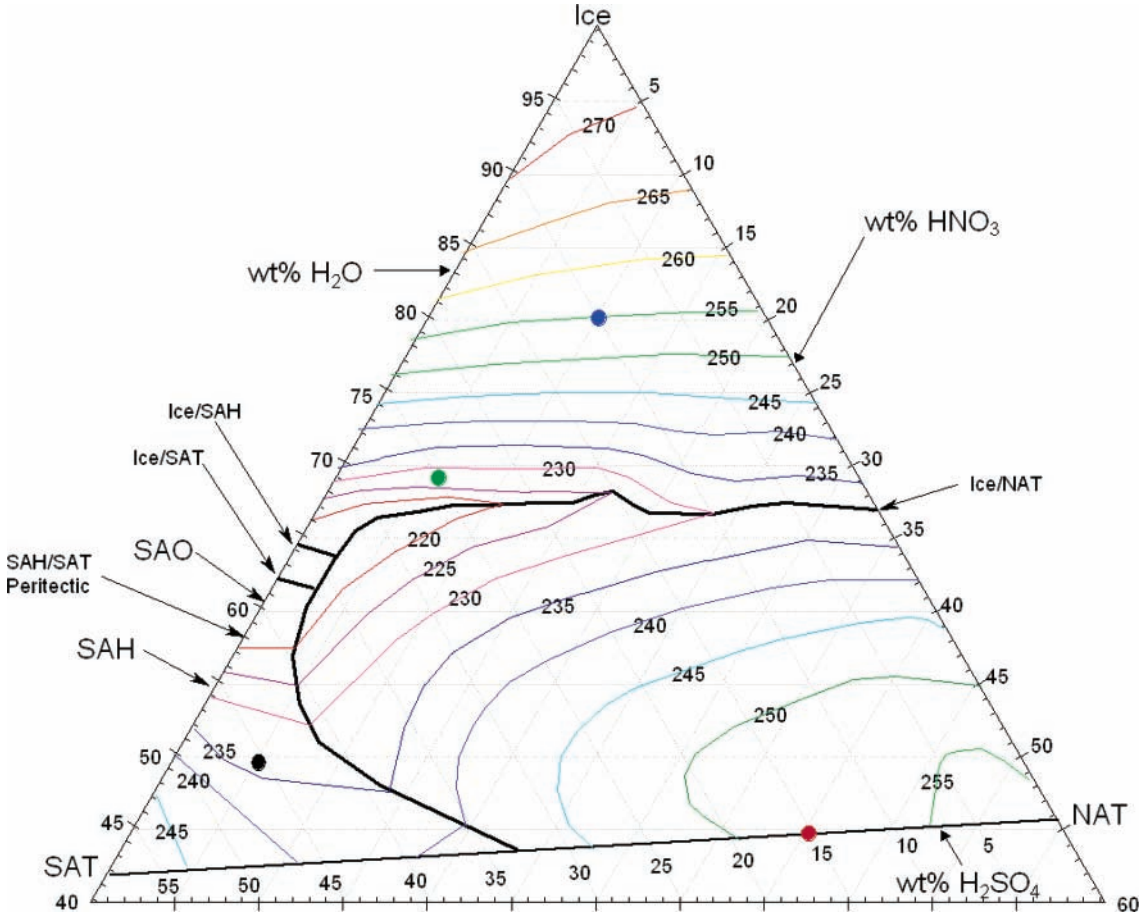

Figure 2. Plot of ice/SAT/NAT region of the ternary $H_2SO_4/HNO_3/H_2O$ phase diagram. The line connecting SAT and NAT compositions is an Alkemade line. The black curve represents the boundary curve compositions as determined from our analysis of melting temperatures. Temperature contours are for final melting temperatures as given in the figure. Dots are color coded and correspond to the concentrations of the respective thermograms in Figure 3.

1.2 K (average of all samples), which we have assigned to the ice/SAT/NAT ternary eutectic melting. Even though this is a thermodynamically metastable eutectic, we detected this transition in nearly every sample (97% of those samples that completely froze), the exception being a few samples along the Alkemade line that represent a SAT/NAT binary system. Examples of this transition are shown in three of the thermograms (black, blue, and green traces) in Figure 3. The composition of the melt at the ice/SAT/NAT eutectic is estimated to be 36 ± 1 wt % H_2SO_4 and 2 ± 1 wt % HNO_3. Thus any completely frozen sample that contains ice, SAT, and NAT in contact with each other will have liquid present at temperatures of 197.4 K and above unless SAT is the first solid to melt at the ternary eutectic. In this case, it is possible that at least some of the liquid could recrystallize into SAH. However, to form SAH from the SAT melt without any liquid remaining, some ice would have to be converted for use in crystallizing SAH.

The total composition of the sample determines which of the three solids melts at the ternary eutectic. We have illustrated an example case in Figure 1. Suppose a sample of composition given by point A in Figure 1 were to completely freeze at a temperature below 197.4 K to form ice, SAT, and NAT in contact with each other. Upon an increase in temperature to 197.4 K, the ternary eutectic point would be reached at point C, whereupon four phases would be in coexistence with zero degrees of freedom according to the Gibbs phase rule: ice, NAT, SAT, and liquid of composition represented by point C. As the temperature continues to increase to just above 197.4 K, all of the SAT will completely melt, and the liquid composition will follow the phase boundary curve from point C to point B as ice and NAT continuously melt. Along the ice/NAT phase boundary, there is one degree of freedom according to the Gibbs phase rule. Thus as temperature is changed, the liquid composition changes following the boundary. When the temperature at point B is reached, the remaining NAT will melt. As temperature increases, the liquid composition will follow the red line in Figure 1 to point A as ice continuously melts. Point A represents the final melting of ice, and thus only liquid exists at higher temperatures for this composition. To determine the location of point B, a line is drawn from the ice apex through point A to the ice/NAT phase boundary. The intersection is the location of point B on the ice/NAT eutectic curve. This process can be followed for a sample of any composition on the diagram; a line is drawn from the apex of the solid in whose primary phase field the total composition lies, through the composition point to the phase field boundary. The order of phases melting is also determined by which region of the diagram a sample's concentration falls. The regions are numbered 1−6 in Figure 1 and are separated by green lines and the phase boundary curves. For example, a sample with total composition of 30/20 H_2SO_4/HNO_3 wt % would fall into region 4 in Figure 1. The sample would begin melting at point C, with ice being the first phase to completely melt. The liquid composition would then follow the phase boundary between the SAT and NAT primary phase fields until the final melting of SAT occurs at point D. The last solid to melt would then be NAT at point E on the diagram. A summary of the order of melting by region in Figure 1 is given in Table 5. The blue thermogram in Figure 3 is typical of most

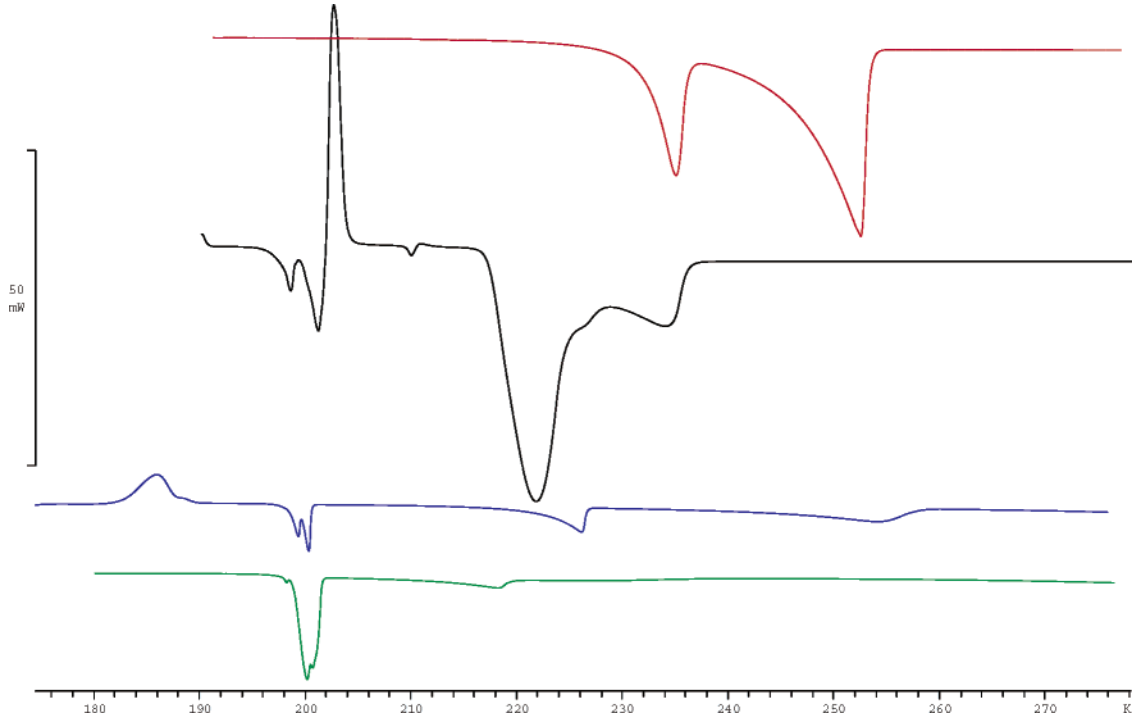

Figure 3. Thermograms for several systems corresponding to colored dots in Figure 2 (exotherms point up): (red) 14.93/39.91 H_2SO_4/HNO_3 wt %, endotherm at 231 K is melting of SAT at the SAT/NAT eutectic, endotherm at 252 K is melting of NAT; (black) 44.4/4.9 H_2SO_4/HNO_3 wt %, endotherm at 198 K is melting of ice at the ice/SAT/NAT ternary eutectic, endotherm at 200 K is the thermal decomposition of SAO, these two transitions are immediately followed by a recrystalization of the melt at 201 K (exotherm), small endotherm at 209 K is the melting of ice at the ice/SAH/NAT ternary eutectic, endotherm at 218 K is the peritectic reaction of SAH → SAT, small endotherm (change in slope) at 225 K is the melting of NAT at the SAT/NAT phase boundary, final endotherm is the melting of SAT; (blue) 10.00/9.97 H_2SO_4/HNO_3 wt %, exotherm at 185 K is a cold crystallization, endotherm at 198 K is melting of SAT at the ternary eutectic, endotherm at 199 K is thermal decomposition of SAO, endotherm at 226 K is melting of NAT at the ice/NAT phase boundary, endotherm at 254 K is melting of ice; (green) 24.61/6.40 H_2SO_4/HNO_3 wt %, small endotherm at 198 K is melting of SAT at the ternary eutectic, endotherm at 200 K is thermal decomposition of SAO, endotherm at 200.5 K is an unassigned transition (see text), endotherm at 218.1 K is melting of NAT at the ice/NAT phase boundary, very small endotherm at 225 K is final melting of ice.

TABLE 1: Phase Boundary Concentrations (wt %) and Temperatures

$[H_2SO_4]$	$[HNO_3]$	$[H_2O]$	T (K)	AIM[a]	difference[b]
		Ice/NAT Phase Boundary			
0.0	33.1	66.9	230.6	230.5	0.1
5.0	27.6	67.4	229.2	230.5	−1.3
10.0	23.8	66.2	229.3	228.5	0.8
13.6	20.0	66.4	228.0	226.5	1.5
15.0	17.1	67.9	223.9	225.6	−1.7
17.9	15.0	67.1	223.9	228	−4.1
20.0	12.9	67.1	222.0	228	−6
23.0	10.0	67.0	221.1	227.5	−6.4
25.0	7.8	67.2	217.7	228	−10.3
30.0	3.8	66.2	213.3	223	−9.7
		SAT/NAT Phase Boundary			
36.2	18.2	45.6	238.8	238.5	0.3
41.2	8.1	50.7	231.9	230	1.9
		Ice/SAT Phase Boundary			
37.9	0.0	62.1	199.3	c	
		Ice/SAH Phase Boundary			
35.7	0.0	64.3	211.3	211.7	0.4

[a] AIM[41] output freezing temperature for concentration listed. This was not necessarily the phase boundary according to the model. [b] AIM temperature subtracted from our temperature. [c] The AIM does not predict this value because it generates solid $H_2SO_4 \cdot 6.5H_2O$ at this composition.

concentrations in this Alkemade region of the phase diagram; the ice, SAT, and NAT melting transitions are clearly seen with the addition of the SAO transition (discussed below).

We observed very few samples (five) that displayed a eutectic transition that we have interpreted to be the ice/SAH/NAT eutectic, even though this eutectic is thermodynamically stable. These samples ranged in composition from 40 to 50 wt % H_2SO_4 and 5 to 15 wt % HNO_3. An example thermogram with this transition is given in Figure 3 (black trace). Clearly this is a region, near the SAH composition (45.6 wt % H_2SO_4) and low HNO_3 composition, where we would expect SAH to be more likely to form. An average of the five samples yields a eutectic temperature of 209.36 ± 0.17 K. Evidence that this is a ternary eutectic is given in the fact that it is below the ice/SAH binary eutectic, which occurs at 211 K. The ternary eutectic temperature of 209 K is reasonable given that a small amount of HNO_3 would be expected to depress the ice/SAH eutectic. The composition of the melt at this eutectic is estimated to be 34 ± 1 wt % H_2SO_4 and 2 ± 1 wt % HNO_3. Therefore, if a completely frozen sample contains ice, SAH, and NAT with no presence of SAT or SAO (to be discussed below), liquid will be present in the sample at temperatures of 209.3 K and above. As indicated by the black thermogram in Figure 3, in some cases a solid will melt at the ice/SAT/NAT eutectic along with SAO; the resulting liquid may then recrystallize into a combination of ice/SAH/NAT. This process was often seen in the H_2SO_4/H_2O binary system experiments[32] and occasionally in the ternary (see black trace in Figure 3).

SAO Stability Regions. We have detected transitions in ternary samples that correspond to the thermal decomposition of SAO (60% of samples that completely froze). An average of all samples that contained this transition yields a decomposition temperature of 199.38 ± 0.97 K, which is a depression of the decomposition point of 1 K from the value of 200.37 ±

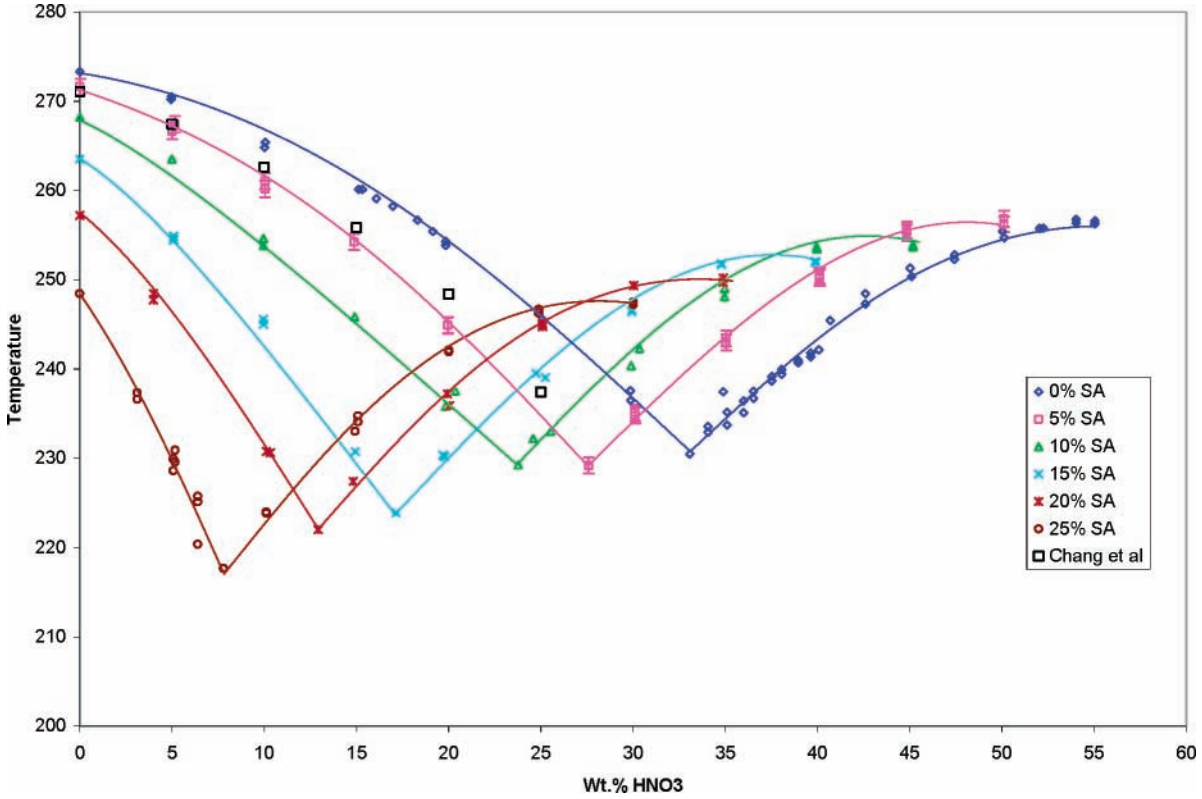

Figure 4. Plot of final melting temperatures of ternary samples as a function of HNO_3 concentration for constant H_2SO_4 concentrations as given in the legend. Data points to the left of the phase boundary represent the melting of ice, and data points to the right of the phase boundary represent the melting of NAT. Data points at the intersection of liquidus curves at each composition of sulfuric acid are calculated phase boundary compositions and temperatures from our analysis (see text). The data of Chang et al. are melting points for solutions of 5 wt % H_2SO_4. Error bars are presented for our 5 wt % H_2SO_4 data. Error bars on the data of Chang et al. are approximately the size of the symbol.

TABLE 2: Melting Point Polynomial Coefficients from Eq 1 in Ice Primary Phase Region[a]

$[HNO_3]$	A_2	A_1	A_0	valid $[H_2SO_4]$
0	−0.0556	0.303	273	0−30
5	−0.0590	−0.119	270	0−25
10	−0.0668	−0.362	265	0−20
15	−0.0592	−1.14	261	0−15
20	−0.0225	−1.60	254	0−10
25		−2.3319	245	0−5

[a] Concentrations of HNO_3 and H_2SO_4 are given in wt %.

TABLE 3: Melting Point Polynomial Coefficients from Eq 1 in NAT Primary Phase Region Using the "NA" Parameterization (See Text)[a]

$[HNO_3]$	A_2	A_1	A_0	valid $[H_2SO_4]$
10	−0.0475	3.68	162	25−40
15	−0.0763	5.03	156	20−40
20	−0.0509	3.13	195	15−30
25	−0.0668	3.27	206	10−30
30	−0.0550	2.30	224	5−25
35	−0.0748	2.35	233	0−20
40	−0.0820	1.79	244	0−15
45	−0.124	1.54	251	0−10

[a] Concentrations of HNO_3 and H_2SO_4 are given in wt %.

0.36 K in the binary H_2SO_4/H_2O system.[32] We have confirmed the identity of this transition by the correlation of DSC and IR experiments where SAO was detected as the major phase with both techniques for samples of the same concentration. The SAO transition is seen in the three thermograms in Figure 3 (black, blue, and green traces). Since this is a thermal decomposition rather than a eutectic melting between two primary phase fields, the transition temperature does not change as a function of sample concentration.[32]

TABLE 4: Melting Point Polynomial Coefficients from Eq 1 in NAT Primary Phase Region Using the "SA" Parameterization (See Text)[a]

$[H_2SO_4]$	A_2	A_1	A_0	Valid $[HNO_3]$
0	−0.0427	4.96	113	35−50
5	−0.0474	4.91	130	30−50
10	−0.0557	5.00	142	25−45
15	−0.0531	4.28	166	20−40
20	−0.0596	4.13	179	15−35
25	−0.0639	3.76	192	10−30
30	−0.0785	3.69	200	5−25

[a] Concentrations of HNO_3 and H_2SO_4 are given in wt %.

TABLE 5: Order of Melting of Phases Corresponding to Regions of the Phase Diagram Given in Figure 1

region in Figure 1	solid that completely melts at ternary eutectic (point C)	second solid to completely melt	final solid to melt
1	NAT	SAT	ice
2	SAT	NAT	ice
3	SAT	Ice	NAT
4	ice	SAT	NAT
5	ice	NAT	SAT
6	NAT	ice	SAT

The amount of a solid present as a fraction of the total mass of sample can be determined using

$$y_i = \frac{EM_i}{\Delta H_i^{\mathrm{fus}} m_{\mathrm{T}}} \tag{2}$$

where y_i is the mass fraction of species i, E is the energy of the transition as measured by the DSC, M_i is the molar mass of

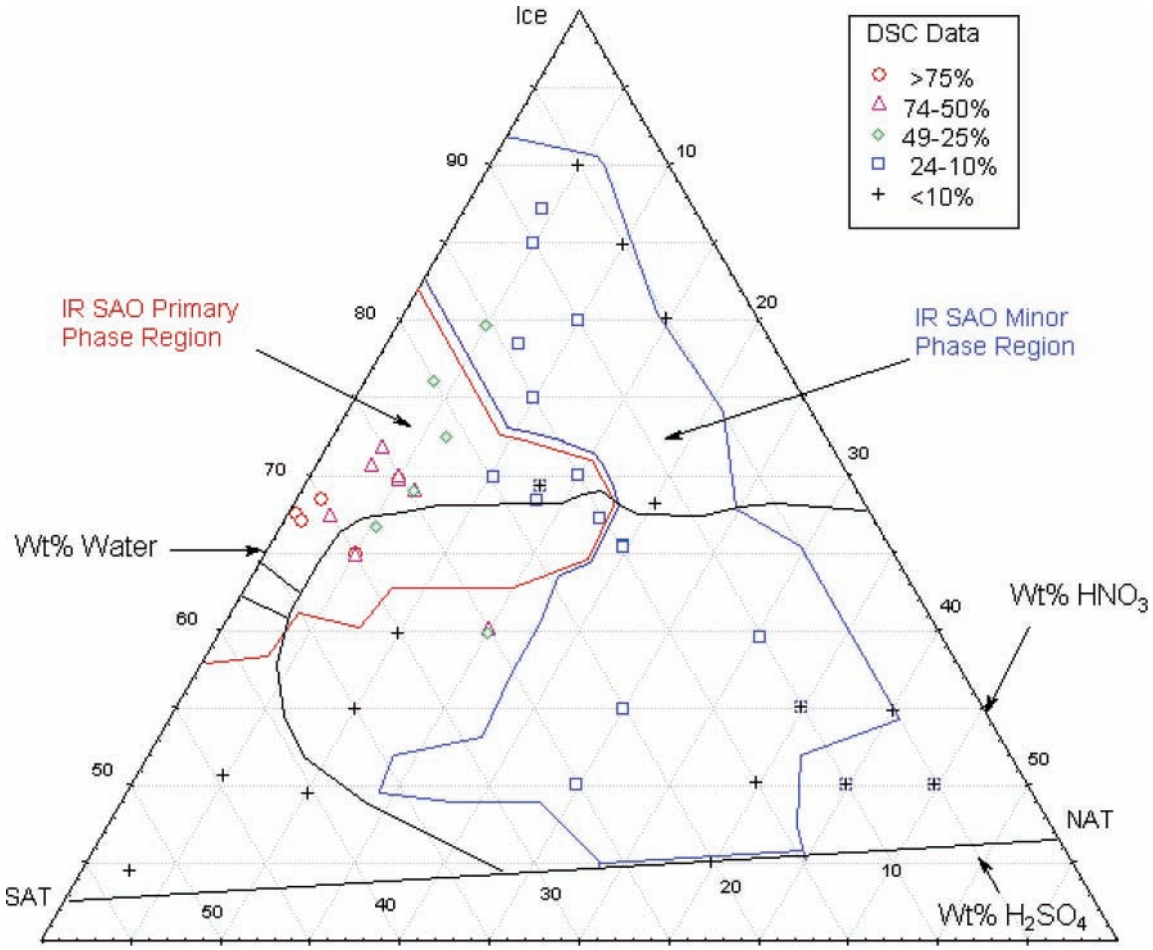

Figure 5. SAO content in frozen ternary samples. Key to DSC content data (percent by mass) is given in the legend. The red line marks regions where SAO was the major phase detected in IR experiments. The blue line is the area in which SAO was detected to be present with other phases in IR experiments. The black lines are the phase boundaries in the diagram that separate the primary phase fields of ice, NAT, and SAT. The black line connecting NAT and SAT compositions is an Alkemade line.

solid i, ΔH_i^{fus} is the molar enthalpy of fusion of species i, and m_T is the total mass of the sample; where i represents SAO, SAT, etc. In the case of SAO, we have used the fusion enthalpy of Beyer et al.[32] to determine the fraction of SAO present in frozen samples. The results are given in Figure 5 along with results from IR experiments. We have labeled a region "IR SAO Primary Phase Region" marking the concentrations where the IR spectra of frozen samples appeared to be entirely due to SAO features. A second region labeled "IR SAO Minor Phase Region" indicates concentrations where we detected features in our IR spectra due to both SAO and another solid (ice, NAT, or SAT). It is seen that there is a strong correlation between the regions of high SAO content as determined by DSC and IR experiments. SAO is a major fraction of the solid mass in a frozen ternary sample in an area between approximately 65−80 wt % water, <20 wt % HNO_3, and 15−35 wt % H_2SO_4. An unexpected result was the observation that SAO is present in samples in the NAT primary phase region even to fairly high HNO_3 and low H_2SO_4 concentrations. In this region, our IR spectra displayed characteristics of both SAO and NAT. An example is shown in Figure 6 where we have compared the spectrum of a frozen 15/25 wt % H_2SO_4/HNO_3 sample with our spectra for pure SAO and NAT. This is in agreement with our DSC data as shown in Figure 5, indicating SAO was <25% of the mass of frozen sample, while (from other analyses) the NAT content was >50% for H_2SO_4 concentrations <15 wt %.

Solid-Phase Content. By use of eq 2 and the enthalpies of fusion, we have determined the content of the solid phase of our frozen DSC samples with respect to both NAT and ice. Content of frozen samples with respect to NAT is given in Figure 7. As expected, the region where NAT is the major solid phase is roughly the same concentration range covered by the NAT primary phase field and becomes an increasing fraction of the solid phase the closer the sample composition is to the NAT composition. NAT also appears as a significant minor phase in a large portion of the ice primary phase field, especially at lower concentrations of H_2SO_4. Content of frozen samples with respect to ice is given in Figure 8. The most noticeable feature here is how little ice is present in frozen samples. This is especially surprising in the ice primary phase field between 15 and 30 wt % H_2SO_4, where most samples contained less than 10% ice by mass. Upon comparison with the SAO content given in Figure 6, it is readily seen that this is an area of high SAO content. As crystals of ice and SAO grow, they compete for water molecules to incorporate into their respective crystal lattices. On the basis of our results, it is likely that SAO grows faster than ice to become a much larger fraction of the solid phase in this region.

New Thermodynamic Transition. We have identified a transition in the DSC experiments that we are unable to assign to any known transition. An example of this transition is given in Figure 3 (green trace). Nine samples had a thermogram signal corresponding to this transition, which occurs at approximately 200 K. Seven of the samples had a concentration within 2 wt % of 25/5 wt % H_2SO_4/HNO_3. If this transition is due to the thermal decomposition of a new solid, then the stoichiometry

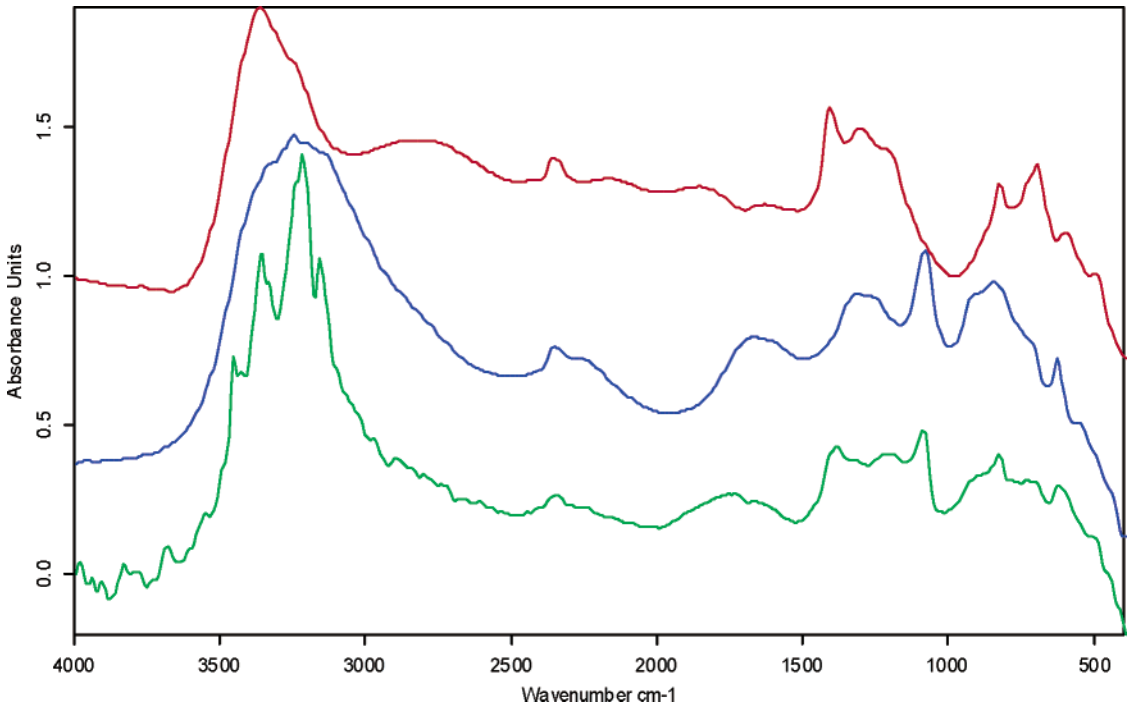

Figure 6. IR spectrum of a frozen 15/25 wt % H_2SO_4/HNO_3 sample (green) showing features of both SAO and NAT. This concentration falls in the NAT primary phase field. Reference spectra of SAO (blue) and NAT (red) are those given in Beyer et al.[32] and Beyer and Hansen,[31] respectively. SAO peaks in common with sample: 1314, 1088, 845, and 626 cm^{-1}; NAT peaks in common with sample: 1403, and 1207 cm^{-1}. Spectra have been offset for clarity.

of the solid can be inferred from the small concentration range of samples that displayed this transition. A composition of $HNO_3 \cdot 3H_2SO_4 \cdot 45H_2O$ has a concentration of 25.2/5.4 wt % H_2SO_4/HNO_3. While the transition was clearly visible in the DSC thermograms, we did not observe unique signatures for this transition in the IR experiments. Thus, if it is a new phase, it is not a significant portion of the frozen solid in our samples. We encourage further investigation of samples in this concentration region to further elucidate evidence for this transition.

Comparison with Literature Data. Carpenter and Lehrman report only final melting points in their work and seem to have estimated the position of eutectic compositions based on minima in their measured temperatures. Their temperature determinations were made by plotting time vs temperature for a melting sample and then determining the point of a change in slope. Obviously this technique is not very sensitive to phase transitions accompanied by relatively small enthalpies. Three different thermometers were used depending on temperature range: mercury, toluene, and pentane, and they estimate their temperature measurements to be better than ±0.6 °C in all regions. Carpenter and Lehrman observed that "crystals could rarely be obtained by merely chilling the mixtures to very low temperatures." Solutions that did not freeze simply by cooling were treated in the following way: "the crystallization, if not spontaneous, was induced by inoculating a supercooled mixture with a crystal obtained by chilling a mixture of the composition of the hydrate sought, or by pouring the supercooled mixture into another mixture of not very different composition, in which crystallization had been induced". A significant problem with this technique is that the seeded phase may not have been the most thermodynamically stable phase under equilibrium conditions, thus potentially altering their construction of the equilibrium phase diagram.

Carpenter and Lehrman did not undertake a systematic study of the phase diagram as a function of concentration of any of the three species, and no clear pattern is discernible in the concentrations they report (in a few cases, they did take a solution and add water to it after each run, thereby creating a set of solutions with a constant ratio of H_2SO_4/HNO_3). We studied solutions of the same concentration as that of Carpenter and Lehrman in the ice primary phase region in order to have a point of comparison between our melting temperatures and theirs. We have found that we observe lower melting points than those of Carpenter and Lehrman for samples of the same concentration. An analysis of 38 samples yielded differences ranging from 1 to 13 K, with an average difference of 4.1 K between our melting points and those of Carpenter and Lehrman. This difference cannot be explained simply by the uncertainty in our temperature measurements or theirs. In general, the larger differences between the data sets are near the ice/NAT phase boundary. This is as would be expected from the technique they were using. Near the phase boundary, the amount of solid present at the final freezing will be very small, most of the solid having already melted at the ternary eutectic and along the phase boundary. Thus, there would have been only a slight change in the slope of a plot of temperature vs time in their experiments, which would increase the error of their measurement of the final melting temperature significantly. Another indication that the melting temperatures of Carpenter and Lehrman contain errors is the observation that the line of maximum melting temperature originating at the binary composition of a molecular solid and extending into the ternary diagram does not follow an Alkemade line in their work. Thus, for example, the temperature maximum lines drawn on their Figure 6 (ternary phase diagram) for NAT and SAT phases do not connect and thus do not constitute an Alkemade line as they must.

There also appears to be errors in their analysis outside the Alkemade region presented in this paper. Since we did not study these areas, we can only point out the errors on a theoretical basis. A region is mapped out for sulfuric acid dihydrate (SAD) in their work based only on three measurements, and the mapped region does not appear to include the stoichiometric ratio of

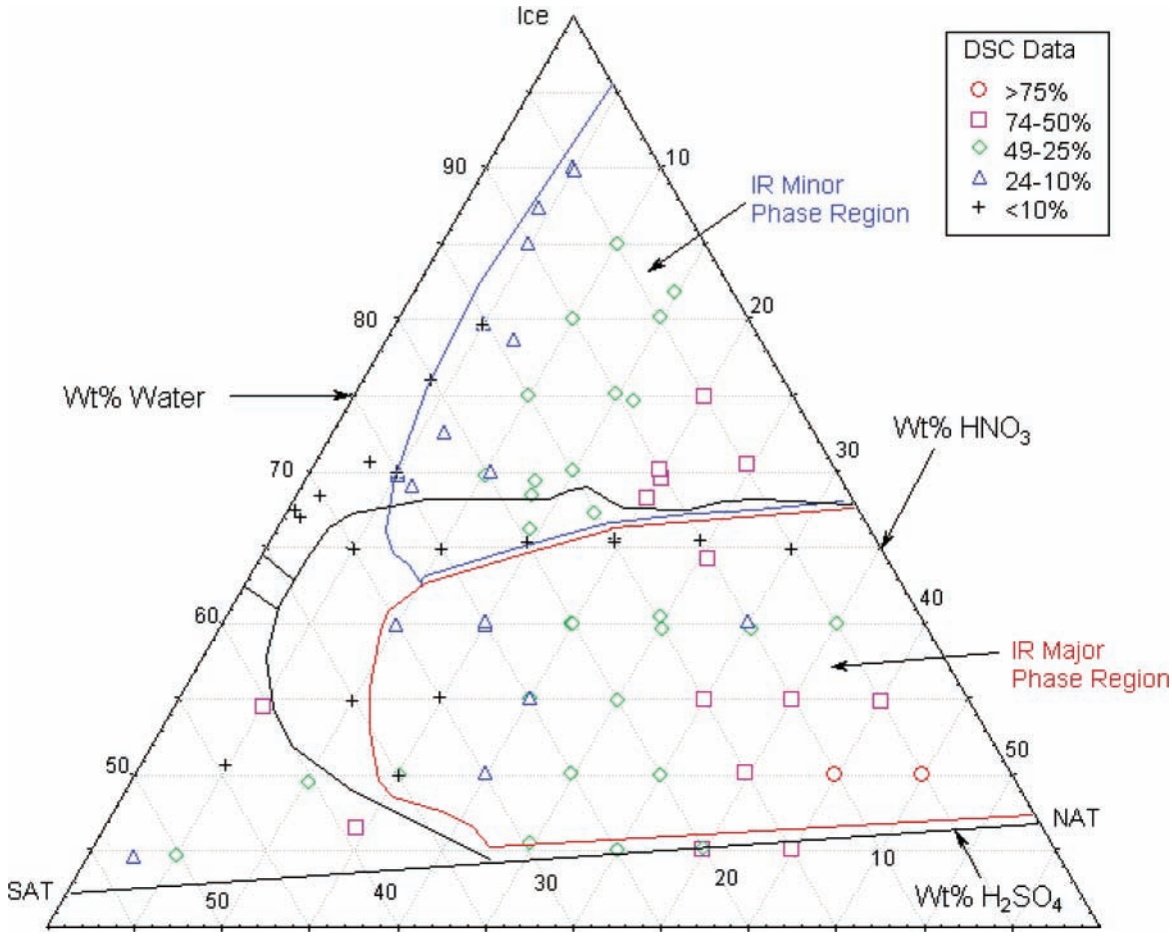

Figure 7. NAT content in frozen ternary samples. Key to DSC content data (percent by mass) is given in the legend. The red line marks region where NAT was the main phase detected in IR experiments. The blue line is the area in which NAT was phase boundaries in the diagram that separate the primary phase fields of ice, NAT, and SAT. The black line connecting NAT and SAT compositions is an Alkemade line.

SAD (33 mol % H_2SO_4) according to their Figure 6. Also, they indicate that SAM is a solid that forms in the binary system H_2SO_4/HNO_3 via the dehydration of HNO_3. However, dehydration of HNO_3 would form N_2O_5, and thus the solid formed would be some combination of SAM and N_2O_5. They do not account for the N_2O_5 that must be in the system.

The final melting points of Chang et al.[22] are plotted in Figure 4 for their solutions with 5 wt % H_2SO_4. They did not report specific temperatures or thermograms in their paper, so we have simply interpolated values from their Figure 6 (phase diagram). While there is good agreement with our data for 0−10 wt % HNO_3 (within the error of our and their temperature data), their melting points are higher than those we report for 15−25 wt % HNO_3 solutions. There are different theories of which point on a thermogram endotherm peak corresponds to the final melting depending according to how the thermogram was acquired and how temperature is reported.[36] We have taken the maximum in the endotherm as the final melt temperature in our thermograms since the Mettler-Toledo DSC thermograms are reported as a function of sample temperature. We do not know how Chang et al. interpreted their thermogram data, or how their DSC software analyzes a melt transition. We do know that the software used in the experiments of Chang et al. reports the program temperature rather than actual sample temperature; however, this is claimed to be very close to the sample temperature.[37,38] That being the case, the final melting point of the last solid present should correspond to the peak of the last endotherm upon heating. We have analyzed the HNO_3/H_2O binary system thermograms reported by Chang et al. in their Figure 5 assuming the peak of the final endotherm corresponds to the final melting of ice for 5−30 wt % HNO_3 samples. Upon comparison with the historical work,[39,40] it is seen that their 5 and 10 wt % samples have a melting temperature 1.5 K below the historical work and the 15−30 wt % samples have a melting temperature 1−6 K above the historical work. We have demonstrated previously that our DSC data in this range are in excellent agreement with the historical work.[31] Therefore, we believe our melting temperatures in the ternary system are more accurate than those reported by Chang et al.

Finally, we have compared our melting points with those generated using the Aerosol Inorganics Model (AIM).[41] Melting points in their model for this system are based on those of Carpenter and Lehrman,[15] and they have demonstrated good agreement between the model output and the values of Carpenter and Lehrman. Thus, as expected, we find similar disagreement between our data and the model output. An analysis of the same 38 samples we analyzed for comparison to the data of Carpenter and Lehrman yielded differences ranging from 0.11 to 14 K, with an average difference of 4.3 K between our melting points and those generated by the model. Again, our measured melting points were generally lower than those of the model. We also compare our phase boundary temperatures to the output of the AIM model as given in Table 1. There is reasonable agreement for the ice/NAT boundary near the ice/NAT binary eutectic; however, as the ternary eutectic is approached along the phase boundary, the AIM deviations from our data become substantial, with our values lower than those predicted by AIM. Also, the concentrations given in the table for the phase boundary from

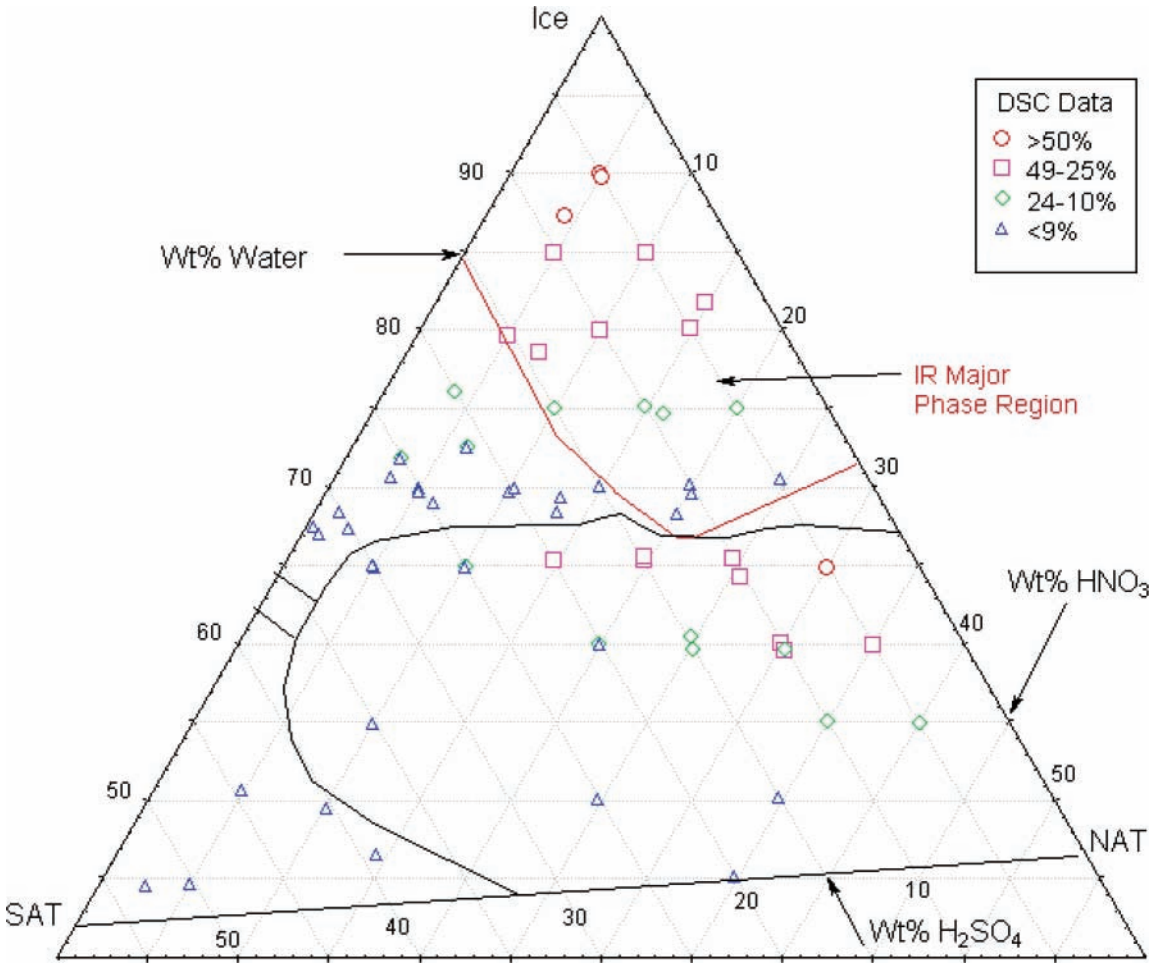

Figure 8. Ice content in frozen ternary samples. Key to DSC content data (percent by mass) is given in the legend. The red line marks region where ice was the main phase detected in IR experiments. The black lines are the phase boundaries in the diagram that separate the primary phase fields of ice, NAT, and SAT. The black line connecting NAT and SAT compositions is an Alkemade line.

our data do not necessarily correspond to the phase boundary concentrations predicted by the model.

Summary

We have undertaken a reinvestigation of the $H_2SO_4/HNO_3/H_2O$ solid/liquid phase diagram in the region of ice/SAT/NAT stability bounded by an Alkemade line connecting the NAT and SAT primary phase fields. We have mapped this region with respect to temperature profiles for the final melting and have parametrized the final melting temperatures as a function of sulfuric and nitric acid concentrations. Our parametrization reproduces the data within our experimental error limits. We have determined the ice/SAT/NAT and ice/SAH/NAT ternary eutectic temperatures and compositions, which can be used to predict the temperature at which melting will occur in completely frozen ternary sample and the composition of the liquid that results. We have also demonstrated how the warming history of a ternary sample can be predicted using the phase diagram.

We have also for the first time mapped the regions of SAO stability in the ternary system and quantified the amount of SAO that can be present in frozen samples. From these results, we determined that SAO can form in samples with a wide range of ternary composition, including samples with significant amounts of HNO_3 present. This indicates that SAO may be much more prevalent in frozen ternary solids than had previously been thought. This solid is easily missed in other types of analyses because of the closeness of its thermal decomposition temperature to the ice/SAT and ice/SAT/NAT eutectic melting temperatures. We have also performed analyses to determine the amount of other major phases (ice and NAT) present in completely frozen ternary samples.

We have compared our results to those of the historic work of Carpenter and Lehrman[15] and find that we observe lower melting points than those of Carpenter and Lehrman for samples of the same concentration with deviations being greatest near the phase boundaries. Given the primitive measurement techniques used by Carpenter and Lehrman, we feel our data are more reliable than theirs. The AIM[41] incorporates the data of Carpenter and Lehrman and, upon comparison of the model output to our data, we find similar discrepancies. In light of these discrepancies we recommend our melting point values be incorporated into atmospheric aerosol models. Our raw data is provided in Table 1S for this purpose.

Finally, we have evidence from our DSC experiments for a new solid that may be a mixed ternary solid in the region of ice/SAH/NAT stability, but the amount of the solid present was too small to detect with IR techniques. Otherwise, the only solids detected in the region studied were those expected: ice, SAT, SAH, SAO, and NAT.

Acknowledgment. We thank an anonymous reviewer for helpful comments on our manuscript. This work was supported by the NSF Atmospheric Chemistry Program (ATM-9911451).

Supporting Information Available: Table 1S contains the experimentally determined melting temperatures for the H_2SO_4/HNO_3/H_2O, HNO_3/H_2O[31] and H_2SO_4/H_2O[32] systems used to create Figure 2. This material is available free of charge via the Internet at http://pubs.acs.org.

References and Notes

(1) Solomon, S. *Rev. Geophys*. **1988**, *26*, 131.
(2) Anderson, J. G.; Toohey, D. W.; Brune, W. H. *Science* **1991**, *251*, 39.
(3) Dessler, A. *The Chemistry and Physics of Stratospheric Ozone*; Academic Press: **2000**.
(4) Wayne, R. *Chemistry of Atmospheres*, 3rd ed.; Oxford University Press: 2000.
(5) Poole, L. R.; McCormick, M. P. *J. Geophys. Res*. **1988**, *93*, 8423.
(6) Hamill, P.; Turco, R. P.; Toon, O. B. *J. Atmos. Chem*. **1988**, *7*, 287.
(7) Wofsy, S. C.; Salawitch, R. J.; McElroy, M. B. *J. Atmos. Sci*. **1990**, *47*, 2004.
(8) Molina, M. J.; Zhang, R.; Wooldridge, P. J.; McMahon, J.; Kim, J. E.; Chang, H. Y. A.; Beyer, K. D. *Science* **1993**, *261*, 1418.
(9) Beyer, K. D.; Seago, S. W.; Chang, H. Y.; Molina, M. J. *Geophys. Res. Lett.* **1994**, *21*, 871.
(10) Voigt, C.; Schreiner, J.; Kohlmann, A.; Zink, P.; Mauersberger, K.; Larsen, N.; Deshler, T.; Kroger, C.; Rosen, J.; Adriani, A.; Cairo, F.; Di Donfrancesco, G.; Viterbini, M.; Ovarlwz, J.; Ovarlez, H.; David, C.; Dornbrack, A. *Science* **2000**, *290*, 1756.
(11) Fahey, D. W.; Gao, R. S.; Carslaw, K. S.; Kettleborough, J.; Popp, P. J.; Northway, M. J.; Holecek, J. C.; Ciciora, S. C.; McLaughlin, R. J.; Thompson, T. L.; Winkler, R. H.; Baumgardner, D. G.; Gandrud, B.; Wennberg, P. O.; Dhaniyala, S.; McKinney, K.; Peter, T.; Salawitch, R. J.; Bui, T. P.; Elkins, J. W.; Webster, C. R.; Atlas, E. L.; Jost, H.; Wilson, J. C.; Herman, R. L.; Kleinbohl, A.; von Konig, M. *Science* **2001**, *291*, 1026.
(12) Northway, M. J.; Gao, R. S.; Popp, P. J.; Holecek, J. C.; Fahey, D. W.; Carslaw, K. S.; Tolbert, M. A.; Lait, L. R.; Dhaniyala, S.; Flagan, R. C.; Wennberg, P. O.; Mahoney, M. J.; Herman, R. L.; Toon, G. C.; Bui, T. P. *J. Geophys. Res.* **2002**, *107* (D20), 8289.
(13) Carslaw, K. S.; Kettleborough, J. A.; Northway, M. J.; Davies, S.; Gao, R.; Fahey, D. W.; Baumgardner, D. G.; Chipperfield, M. P.; Kleinbohl, A. *J. Geophys. Res.* **2002**, *107* (D20), 8300.
(14) DeMore, W. B.; Sander, S. P.; Golden, D. M.; Hampson, R. F.; Kurylo, M. J.; Howard, C. J.; Ravishankara, A. R.; Kolb, C. E.; Molina, M. J. *Chemical Kinetics and Photochemical Data for Use in Stratospheric Modeling*; JPL Publication 97-4, 1997.
(15) Carpenter, C. D.; Lehrman, A. *Trans. AIChE* **1925**, *17*, 35.
(16) Hulsmann, O.; Biltz, W. *Z. Anorg. Allg. Chem*. **1934**, *218*, 369.
(17) Hornung, E. W.; Brackett, T. E.; Giauque, W. F. *J. Am. Chem. Soc.* **1956**, *78*, 5747.
(18) Gable, C. M.; Betz, H. F.; Maron, S. H. *J. Am. Chem. Soc*. **1950**, *72*, 1445.
(19) Ritzhaupt, G.; Devlin, J. P. *J. Phys. Chem*. **1991**, *95*, 90.
(20) Tolbert, M. A.; Middlebrook, A. M. *J. Geophys. Res.* **1990**, *95*, 22423.
(21) Holmes, W. C. *J. Ind. Eng. Chem*. **1920**, *12*, 781.
(22) Chang, H. Y.; Koop, T.; Molina, L. T.; Molina, M. J. *J. Phys. Chem. A* **1999**, *103*, 2673.
(23) Fox. L. E.; Worsnop, D. R.; Zahniser, M. S.; Wofsy, S. C. *Science* **1995**, *267*, 351.
(24) Song, N. *Geophys. Res. Lett.* **1994**, *21*, 2709.
(25) Koop, T.; Biermann, U. M.; Raber, W.; Luo, B. P.; Crutzen, P. J.; Peter, T. *Geophys. Res. Lett.* **1995**, *22*, 917.
(26) Biermann, U. M.; Presper, T.; Koop, T.; Mossinger, J.; Crutzen, P. J.; Peter, T. *Geophys. Res. Lett.* **1996**, *23*, 1693.
(27) Anthony, S. E.; Onasch, T. B.; Tisdale, R. T.; Disselkamp, R. S.; Tolbert, M. A. *J. Geophys. Res.* **1997**, *102*, 10777.
(28) Koop, T.; Luo, B.; Biermann, U. M.; Crutzen, P. J.; Peter, T. *J. Phys. Chem. A* **1997**, *101*, 1117.
(29) Ehlers, E. G. *The Interpretation of Geological Phase Diagrams*; Dover: Mineola, NY, 1972.
(30) Carslaw, K. S.; Clegg, S. L.; Brimblecombe, P. *J. Phys. Chem.* **1995**, *99*, 11557.
(31) Beyer, K. D.; Hansen, A. R. *J. Phys. Chem. A* **2002**, *106*, 10275.
(32) Beyer, K. D.; Hansen, A. R.; Poston, M. *J. Phys. Chem. A* **2003**, *107*, 2025.
(33) *CRC Handbook of Chemistry and Physics*, 74th ed.; Lide, D. R., Ed.; CRC Press: Boca Raton, 1993; 3−208, 351, and 6−58.
(34) Zeleznik, F. J. *J. Phys. Chem. Ref. Data* **1991**, *20*, 1157.
(35) Schubnell, M. *J. Therm. Anal. Calorim.* **2000**, *61*, 91.
(36) Wendlant, W. *Thermal Analysis*, 3rd ed.; Wiley: New York, 1986; 213−216.
(37) Koop, T. Private communication, 2003.
(38) Sichina, B. Thermal analysis list-serve discussion, 2003.
(39) Pickering, S. U. *J. Chem. Soc*. **1893**, *63*, 436.
(40) Kuster, F. W.; Kremann, R. *Z. Anorg. Chem*. **1904**, *41*, 1, 1904.
(41) Carslaw, K. S.; Clegg, S. L.; Brimblecombe, P. *J. Phys. Chem.* **1995**, *99*, 11557−11574.